Research in Astronomy and Astrophysics, 22:105004 (10pp), 2022 October https://doi.org/10.1088/1674-4527/ac8b5b

The Stellar Abundances and Galactic Evolution Survey: Photonic Passbands and Extinction Coefficients for the *u* and *v* Bands

Ke-Feng Tan[1], Gang Zhao[1,2], Zhou Fan[1,2], Wei Wang[1,3], Hai-Bo Yuan[4], Jie Zheng[1], Chun Li[1], Nan Song[5], and Jing-Kun Zhao[1]
[1] CAS Key Laboratory of Optical Astronomy, National Astronomical Observatories, Chinese Academy of Sciences, Beijing 100101, China
tan@nao.cas.cn, gzhao@nao.cas.cn
[2] School of Astronomy and Space Science, University of Chinese Academy of Sciences, Beijing 100049, China
[3] Chinese Academy of Sciences South America Center for Astronomy, National Astronomical Observatories, Chinese Academy of Sciences, Beijing 100101, China
[4] Department of Astronomy, Beijing Normal University, Beijing 100875, China
[5] China Science and Technology Museum, Beijing 100101, China
Received 2021 December 28; revised 2022 July 15; accepted 2022 July 30; published 2022 September 16

Abstract

The Stellar Abundances and Galactic Evolution Survey (SAGES) is a multi-band photometric survey focused on estimation of stellar atmospheric parameters and interstellar extinction. In this paper we have derived photonic passbands for the intermediate-band *u* and *v* filters of the SAGES photometric system. The derived photonic passbands have been compared with those of the *u* and *v* filters of the Strömgren and SkyMapper systems. Synthetic photometry based on the derived photonic passbands could reproduce the observations very well. We have also derived observed, model-free extinction coefficients for the SAGES *u* and *v* bands (as well as the Pan-STARRS *grizy* bands) using the "standard pair" method. The derived reddening coefficients have been compared with those predicted by the extinction laws. Variations of reddening coefficients with effective temperatures and color excesses of *B–V* given by Schlegel et al. ($E(B-V)_{\rm SFD}$) have been investigated. No obvious trends or significant variations with effective temperatures have been found, but reddening coefficients for all the colors exhibit declining trends with increasing $E(B-V)_{\rm SFD}$, with typical relative variations of twenty-some percent from $E(B-V)_{\rm SFD} \sim 0$ to 1.

Key words: stars: general – (ISM:) dust – extinction – techniques: photometric

1. Introduction

The Stellar Abundances and Galactic Evolution Survey (SAGES; Wang et al. 2014; Fan et al. 2018; Zheng et al. 2018, 2019) is a multi-band photometric survey covering ∼10,000 square degrees of the northern sky with a 5σ detection limit of ∼20 mag in the *V* band. The main purpose of the survey is to obtain stellar atmospheric parameters (effective temperature, surface gravity and metallicity) and interstellar extinction using a photometric system consisting of *u*, *v*, *g*, *r*, *i*, *DDO*51, $H\alpha_w$ and $H\alpha_n$ filters.

The SAGES *u* filter (manufactured by Omega Optical, LLC in the US) emulates the Strömgren *u* band (Strömgren 1966), which has good temperature sensitivity for hot stars and good gravity sensitivity for A, F and G stars. The SAGES *v* filter (manufactured by Asahi Spectra Co., Ltd. in Japan) is specially designed to cover the Ca II H & K doublet, which is a good proxy for metallicity. Observations for the *u* and *v* bands have been done with the 90-inch (2.3 m) Bok Telescope on Kitt Peak operated by Steward Observatory of the University of Arizona, and the data have been reduced and internally released (SAGES DR1; Z. Fan et al. 2022, in preparation).

Knowledge of photometric systems, e.g., photonic passbands (system response functions) and extinction coefficients is essential to making full use of the photometric data. In this paper, we present the SAGES *u* and *v* photonic passbands in Section 2, and derive observed, model-free extinction coefficients for the SAGES *u* and *v* bands in Section 3. A brief summary is given in the last section.

2. Photonic Passbands

2.1. The SAGES u and v Photonic Passbands

Photonic passbands for the SAGES *u* and *v* bands were derived by convolving the filter transmissions with the CCD quantum efficiency as well as the atmospheric transmission (one air mass).[6] The mirror reflectivity was neglected. Table 1 gives the normalized SAGES *u* and *v* photonic passbands (S_λ) at 10-Å intervals.

In Table 2, we list three basic parameters for the SAGES *u* and *v* bands, including the mean wavelength ($\lambda_{\rm mean}$), the pivot wavelength ($\lambda_{\rm pivot}$) and the full width at half maximum

[6] The filter transmissions were measured in laboratories by the manufacturers. The CCD quantum efficiency was adopted from the manual of the Bok Telescope. The atmospheric transmission of Kitt Peak was adopted from the KPNO extinction table distributed with IRAF.

(FWHM), where

$$\lambda_{\rm mean} = \frac{\int S_\lambda \lambda d\lambda}{\int S_\lambda d\lambda} \tag{1}$$

and

$$\lambda_{\rm pivot} = \sqrt{\frac{\int S_\lambda \lambda d\lambda}{\int S_\lambda d\lambda/\lambda}}. \tag{2}$$

2.2. Comparison with the Strömgren and SkyMapper Systems

For comparison, we also list in Table 2 the corresponding parameters for the u and v bands of the Strömgren and SkyMapper (Keller et al. 2007) systems, which were calculated based on the photonic passbands from Bessell (2011) and Bessell et al. (2011), respectively. It is clear that the SAGES u band has very similar characteristic wavelengths to the Strömgren/SkyMapper u bands, but its bandwidth is the narrowest among the three bands. For the v bands, both the characteristic wavelengths and bandwidth of the SAGES system are in between those of the Strömgren and SkyMapper systems. The above-mentioned similarities and differences between the SAGES and the Strömgren/SkyMapper u and v bands can also be seen in Figure 1, which plots the normalized u and v photonic passbands of the three systems.

In order to quantify the differences in the u and v bands between the SAGES and the Strömgren/SkyMapper systems, we calculated synthetic u and v magnitudes for the three systems based on the empirical spectra from the INGS[7] library. As reference, synthetic $G_{\rm BP}$ and $G_{\rm RP}$ magnitudes of the Gaia (Gaia Collaboration et al. 2016) photometric system were also calculated following Evans et al. (2018). In Figure 2, the differences in synthetic u and v magnitudes between SAGES and Strömgren/SkyMapper are plotted against $G_{\rm BP} - G_{\rm RP}$; dwarfs and giants are distinguished by color. It is clear that the SAGES u magnitudes are very close to the Strömgren u magnitudes (differing by no more than 0.07 mag), while the differences between the SAGES u magnitudes and the SkyMapper u magnitudes are a bit larger, but still within 0.1 mag for most of the stars. For the v magnitudes, the differences between SAGES and Strömgren/SkyMapper are much more significant (as high as 0.8 and 0.5 mag, respectively) as anticipated.

[7] INGS is a compendium of 143 stellar-type spectra formed from spectra of stars of similar type from IUE, NGSL, and SpeX/IRTF data (https://lco.global/~apickles/INGS/). It is an update of the previous Pickles (1998) library.

Table 1
Normalized SAGES u and v Photonic Passbands

u		v	
λ (Å)	S_λ	λ (Å)	S_λ
3270	0.000	3710	0.000
3280	0.001	3720	0.001
3290	0.003	3730	0.001
3300	0.008	3740	0.002
3310	0.023	3750	0.003
3320	0.073	3760	0.006
3330	0.216	3770	0.011
3340	0.463	3780	0.024
3350	0.666	3790	0.057
3360	0.758	3800	0.145
3370	0.780	3810	0.327
3380	0.776	3820	0.560
3390	0.768	3830	0.738
3400	0.778	3840	0.855
3410	0.813	3850	0.908
3420	0.853	3860	0.912
3430	0.897	3870	0.905
3440	0.930	3880	0.910
3450	0.939	3890	0.924
3460	0.949	3900	0.932
3470	0.959	3910	0.929
3480	0.966	3920	0.926
3490	0.949	3930	0.931
3500	0.970	3940	0.949
3510	0.989	3950	0.967
3520	0.999	3960	0.979
3530	0.995	3970	0.979
3540	0.979	3980	0.977
3550	0.955	3990	0.977
3560	0.926	4000	0.983
3570	0.906	4010	0.992
3580	0.888	4020	0.999
3590	0.876	4030	1.000
3600	0.863	4040	0.996
3610	0.842	4050	0.989
3620	0.799	4060	0.977
3630	0.708	4070	0.927
3640	0.558	4080	0.790
3650	0.375	4090	0.557
3660	0.215	4100	0.321
3670	0.112	4110	0.162
3680	0.056	4120	0.078
3690	0.028	4130	0.040
3700	0.014	4140	0.021
3710	0.008	4150	0.011
3720	0.004	4160	0.007
3730	0.002	4170	0.004
3740	0.001	4180	0.003
3750	0.001	4190	0.002
3760	0.000	4200	0.001
…	…	4210	0.001
…	…	4220	0.000

2.3. Validity of the Photonic Passbands

Knowledge of photonic passbands is essential for synthetic photometry, and its validity must be verified by comparing synthetic photometry based on the derived photonic passbands with actual observations. The most direct way to verify the SAGES u and v photonic passbands is to calculate synthetic

Table 2
Parameters of the SAGES *u* and *v* Bands Compared with those of the Strömgren and SkyMapper Systems

Band	$\lambda_{\rm mean}$ (Å)	$\lambda_{\rm pivot}$ (Å)	FWHM (Å)
SAGES *u*	3496	3495	302
Strömgren *u*	3481	3479	350
SkyMapper *u*	3497	3493	430
SAGES *v*	3958	3957	275
Strömgren *v*	4109	4108	196
SkyMapper *v*	3838	3836	307

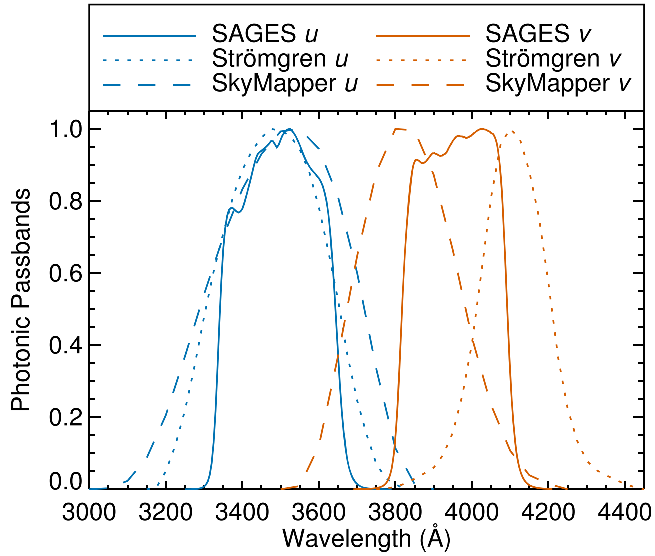

Figure 1. Normalized *u* and *v* photonic passbands of the SAGES system compared with those of the Strömgren and SkyMapper systems.

magnitudes based on spectra with accurate absolute flux calibrations and compare them with the observational *u* and *v* magnitudes from SAGES. Unfortunately, there are very few stars having both observational SAGES magnitudes and spectra with accurate absolute flux calibrations covering the SAGES *u* and *v* bands. This is not unexpected because the SAGES stars are relatively faint, for which spectra with accurate absolute flux calibrations are not easy to acquire, especially in the SAGES *u* and *v* bands. Therefore, we adopted a compromise approach to verify the SAGES *u* and *v* photonic passbands, i.e., by comparisons of synthetic/hybrid color–color diagrams with the observed ones. This method needs to introduce additional photometric systems as reference. Given its unprecedented photometric accuracy and well-defined photonic passbands, the Gaia photometry ($G_{\rm BP}$ and $G_{\rm RP}$ magnitudes) was adopted here as reference.

We first cross-matched the SAGES DR1 catalog with the Gaia DR2 (Gaia Collaboration et al. 2018) catalog to produce a sample with observational *u*, *v*, $G_{\rm BP}$ and $G_{\rm RP}$ magnitudes. Then the following constraints were placed on the sample to obtain reliable observed color–color diagrams:

1. uncertainties of *u*, *v*, $G_{\rm BP}$ and $G_{\rm RP}$ magnitudes are smaller than 0.05 mag (good quality of photometry);
2. $E(B-V)$ estimated by the dust map of Schlegel et al. (1998, SFD) (hereafter $E(B-V)_{\rm SFD}$) is smaller than 0.03 mag (minimal effects of interstellar reddening).

Synthetic/hybrid color–color diagrams used for comparison were constructed based on the INGS and the Next Generation Spectral Library[8] (NGSL; Gregg et al. 2006; Heap & Lindler 2007), both of which contain stellar spectra with accurate absolute flux calibrations. In the INGS library, each spectrum is a combination of spectra from different (but of similar type) stars, so synthetic magnitudes had to be calculated for all of the four bands (*u*, *v*, $G_{\rm BP}$ and $G_{\rm RP}$) involved, and this was made possible by the extensive wavelength coverage of the INGS spectra. As for the NGSL library, the spectral range does not cover the red end of the $G_{\rm RP}$ band. Fortunately, for most of the sample stars, observational $G_{\rm BP}$ and $G_{\rm RP}$ magnitudes can be extracted from the Gaia DR2 catalog, so we only needed to calculate synthetic magnitudes for the *u* and *v* bands. That is why the color–color diagrams based on the INGS and NGSL libraries are referred to as synthetic and hybrid color–color diagrams, respectively.

Now both the observed and synthetic/hybrid color–color diagrams are ready for comparison. Considering that the loci of stars in the color–color diagram are dependent on their atmospheric parameters, the comparison should be restricted to a particular range of stellar parameters, so that the stellar loci would be as slim as possible and thus the comparison would be more convincing. We extracted stellar parameters from the Large Sky Area Multi-Object Fiber Spectroscopic Telescope (LAMOST; Cui et al. 2012; Zhao et al. 2006, 2012) DR7 catalog for the SAGES sample. For the NGSL stars, the stellar parameters determined by Koleva & Vazdekis (2012) were adopted. As for the INGS library, we adopted the effective temperature, metallicity and luminosity class assigned to each spectrum by A. J. Pickles. After investigating the distributions of the stellar parameters, the range $0\,{\rm dex} \leqslant {\rm [Fe/H]} \leqslant 0.2\,{\rm dex}$ and $\log g > 4$ dex (luminosity class of V for the INGS sample) was selected because the number of stars in the NGSL and INGS samples peaks in this range, and an interval of 0.2 dex in [Fe/H] is comparable to the typical uncertainty of metallicity.

Figure 3 features the comparison of color–color diagrams among SAGES, INGS and NGSL samples with $0\,{\rm dex} \leqslant {\rm [Fe/H]} \leqslant 0.2\,{\rm dex}$ and $\log g > 4$ dex. It can be seen that the SAGES

[8] NGSL consists of 379 flux-calibrated stellar spectra observed by Hubble's Space Telescope Imaging Spectrograph (STIS). All the spectra were observed in the same way with a wavelength coverage of 1800–10,100 Å at a resolving power $R \sim 1000$ (https://archive.stsci.edu/prepds/stisngsl/index.html).

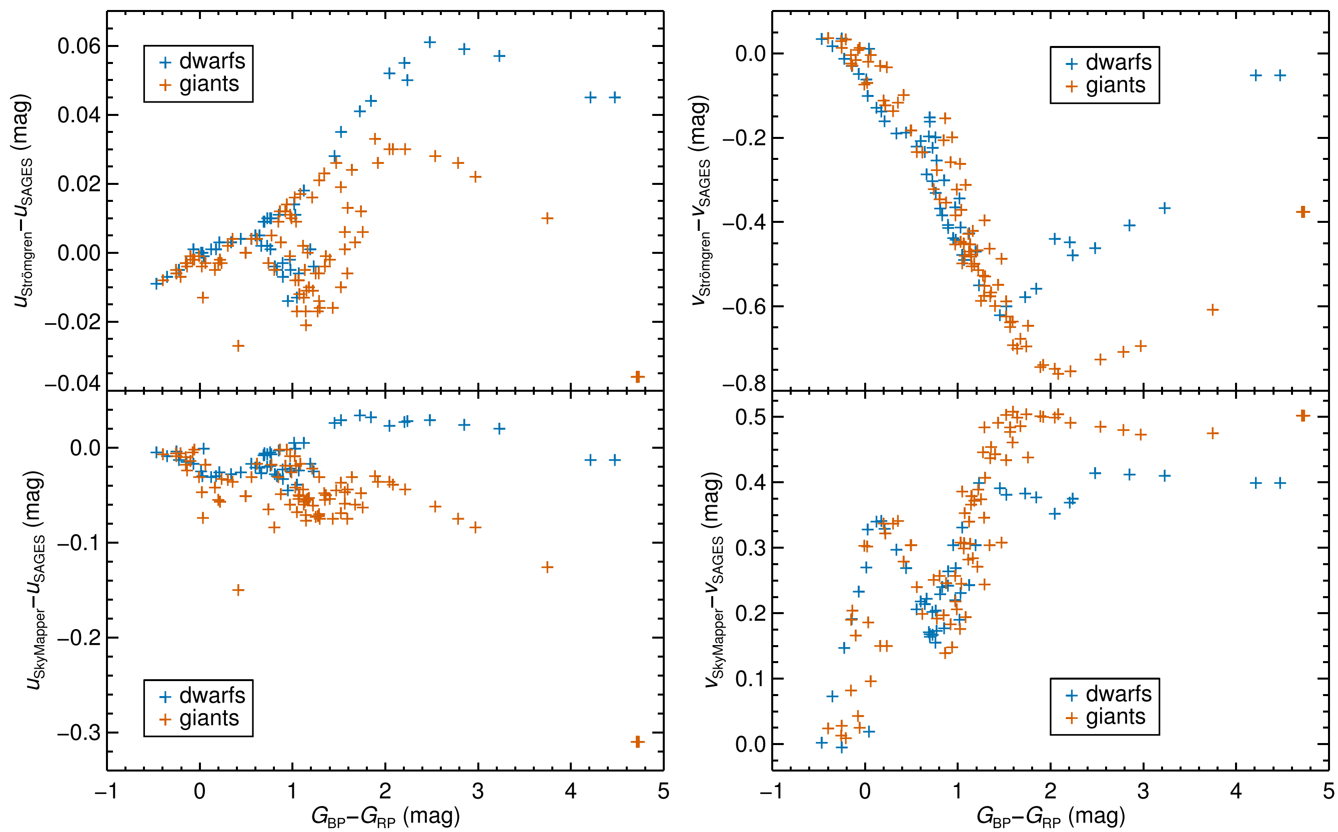

Figure 2. Differences in synthetic u and v magnitudes between SAGES and Strömgren/SkyMapper based on the empirical spectra from the INGS library.

stars (black dots) define clear and slim observed loci in both the $u-G_{\rm BP}$ versus $G_{\rm BP}-G_{\rm RP}$ (upper left panel) and $v-G_{\rm BP}$ versus $G_{\rm BP}-G_{\rm RP}$ (upper right panel) spaces, though there are some outliers which could be due to variations in brightness or photometric uncertainties. The average widths (FWHM) of the $u-G_{\rm BP}$ and $v-G_{\rm BP}$ colors are 0.097 and 0.064 mag, respectively, which correspond to the standard deviations ($\sigma \simeq$ FWHM/2.355 for a Gaussian distribution) of 0.041 and 0.027 mag. The dispersions are dominated by the spread of [Fe/H] and their associated uncertainties, which totally contribute 0.039 and 0.025 mag to the $u-G_{\rm BP}$ and $v-G_{\rm BP}$ colors, respectively. The rest of the scatters could be explained by photometric errors (of the order of 0.01 mag), uncertainties of interstellar reddening, binary stars, etc. The INGS (diamonds) and NGSL (pluses) samples match the observed loci very well except for three outliers (marked with open circles in the plots). For the outlier from the NGSL sample (HD 22049), its synthetic $G_{\rm BP}$ magnitude is 0.07 mag smaller than the observed value, which indicates that the flux of the NGSL spectra for this star might be overestimated in the blue end, and the synthetic u and v magnitudes might also be smaller than the true values. When the synthetic $G_{\rm BP}$ magnitude is adopted in calculating $u-G_{\rm BP}$ and $v-G_{\rm BP}$ colors for this star, the effects partially canceled out and it becomes normal in the color–color diagrams. As for the two outliers from the INGS sample, one (ings_029_g2v, $G_{\rm BP}-G_{\rm RP} \sim 1$) obviously deviates from the general $T_{\rm eff}$ versus $G_{\rm BP}-G_{\rm RP}$ relationship defined by the majority of the stars, while the other one (ings_039_k2v, $G_{\rm BP}-G_{\rm RP} \sim 1.2$) has obviously higher relative flux below 4300 Å compared to the observed NGSL spectra of HD 160346 which has very similar effective temperature, metallicity and $G_{\rm BP}-G_{\rm RP}$ color. The lower panels of Figure 3 quantify the offsets of $u-G_{\rm BP}$ and $v-G_{\rm BP}$ colors between SAGES and INGS/NGSL samples, which show no systematic deviations or dependences on $G_{\rm BP}-G_{\rm RP}$ color. This indicates that the adopted photonic passbands for the SAGES u and v bands could reproduce the observations very well.

3. Extinction Coefficients

When using photometric data, interstellar extinction must be taken into account, especially for those at shorter wavelengths such as the SAGES u and v bands. For a given band a, its extinction coefficient R_a is defined as $R_a = A_a/E(B-V)$, where A_a is the total extinction for band a and $E(B-V)$ is the color excess of B–V. Similarly, the reddening coefficient

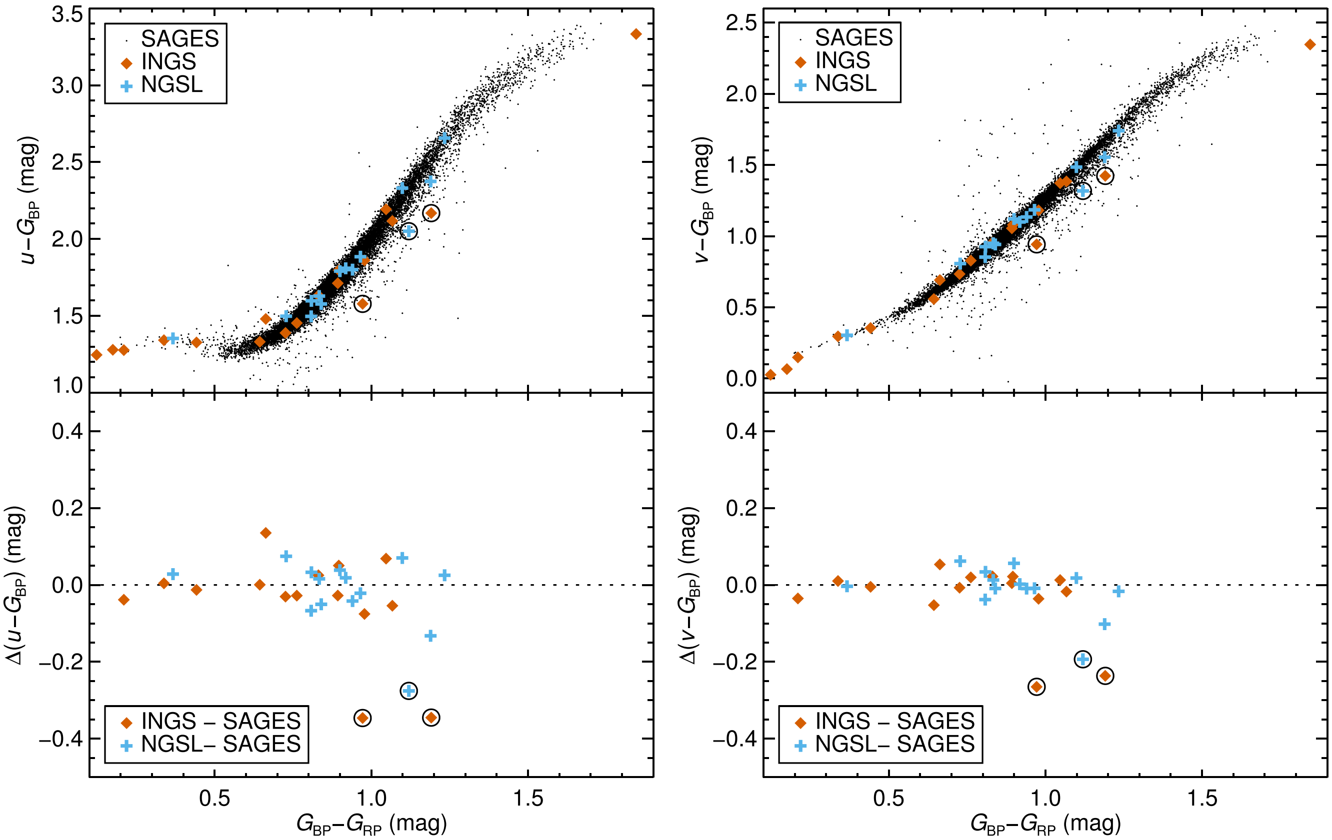

Figure 3. Upper panels: color–color diagrams of SAGES (observed), INGS (synthetic) and NGSL (hybrid) samples with 0 dex $\leqslant$ [Fe/H] $\leqslant$ 0.2 dex and $\log g > 4$ dex. Lower panels: offsets of $u - G_{BP}$ and $v - G_{BP}$ colors between SAGES and INGS/NGSL samples. For the SAGES sample, the median values of $u - G_{BP}$ and $v - G_{BP}$ in bins of 0.03 mag around the $G_{BP} - G_{RP}$ of the INGS/NGSL samples (if available) were adopted when calculating the offsets. Three outliers that obviously deviate from the general trends are marked with open circles.

for a given color $a-b$ could be expressed as $R_{a-b} = R_a - R_b = (A_a - A_b)/E(B-V) = E(a-b)/E(B-V)$. Extinction coefficients could be computed from an extinction curve in combination with the photonic passbands and a source spectrum. However, this method depends on the adopted extinction curve, which could be different from study to study. In this work, we utilized the "standard pair" technique (Yuan et al. 2013) to derive model-free extinction coefficients. As the SAGES u and v bands were devised to be used together with the photometric data of the Panoramic Survey Telescope and Rapid Response System (Pan-STARRS; Chambers et al. 2016), for the convenience of users, we computed extinction coefficients not only for the SAGES u and v bands but also for the Pan-STARRS g, r, i, z and y bands.

3.1. Method and Results

As described in Yuan et al. (2013), the "standard pair" method requires a target sample of stars suffering from significant interstellar extinction and a control sample of stars with similar spectral types but negligible reddening which are used to estimate the intrinsic colors of the target stars. We first performed a cross-match between the SAGES DR1, the Pan-STARRS DR1 (Flewelling et al. 2020), the AAVSO Photometric All-Sky Survey (APASS; Henden et al. 2009) DR9 and the LAMOST DR7 catalogs to get a sample of stars with SAGES u and v, Pan-STARRS g, r, i, z and y, and Johnson B and V magnitudes, as well as stellar atmospheric parameters ($T_{\rm eff}$, $\log g$ and [Fe/H]). Then stars satisfying the following criteria:

1. uncertainties of u, v, g, r, i, z, y, B and V magnitudes are smaller than 0.1 mag;
2. uncertainties of $T_{\rm eff}$, $\log g$ and [Fe/H] are smaller than 100 K, 0.2 dex and 0.1 dex, respectively;
3. $E(B-V)_{\rm SFD} > 0.1$ mag;

were selected as the target stars. For the control stars, the selection criteria were the same as for the target stars except the last one which changed to $E(B-V)_{\rm SFD} < 0.03$ mag. Finally, 77,984 target stars and 39,143 control stars were selected.

For each target star, stars from the control sample with differences in $T_{\rm eff}$, $\log g$ and [Fe/H] smaller than 100 K, 0.2 dex and 0.1 dex, respectively, were selected as its pair stars. Only those target stars with more than 10 pair stars were used for the following determination of reddening coefficients. The paired control stars were first corrected for interstellar reddening using $E(B-V)_{\rm SFD}$ and an initial set of reddening coefficients based on Schlafly & Finkbeiner (2011). Then their dereddened colors were used to estimate the intrinsic colors of the target star assuming that the intrinsic colors vary linearly with $T_{\rm eff}$, $\log g$ and [Fe/H] in small ranges. The differences between the observed and intrinsic colors (i.e., color excesses) for the target stars were then compared to $E(B-V)_{\rm SFD}$ to derive a new set of reddening coefficients. Figure 4 depicts the derived color excesses of various colors as a function of $E(B-V)_{\rm SFD}$ for the target stars. The data points within the range $0.1\ {\rm mag} < E(B-V)_{\rm SFD} < 0.7$ mag were binned into six groups with a bin size of 0.1 mag, and the median value of each group is signified with a vermilion plus in the plot. Reddening coefficient for each color was derived by fitting the six median points to the linear model $y = ax$ with minimized chi-square error statistic. The above processes were iterated until the derived reddening coefficients do not change. The vermilion line plotted in Figure 4 represents the final linear fit result, and the slope (i.e., reddening coefficient) and associated uncertainty are marked at the bottom right of each panel. To measure the goodness of the linear fits, the coefficients of determination (R^2) were calculated. For all the colors, the R^2 values are greater than 0.98, which indicates that the derived linear models are pretty robust.

Note that the reddening coefficients displayed in Figure 4 are relative to $E(B-V)_{\rm SFD}$, which is claimed to be overestimated by previous studies (Schlafly et al. 2010; Schlafly & Finkbeiner 2011; Yuan et al. 2013 and references therein). This is also confirmed by our results as shown in the bottom right panel of Figure 4, which indicates that $E(B-V) = 0.78E(B-V)_{\rm SFD}$. Therefore, the reddening coefficients derived in Figure 4 should only be used in combination with $E(B-V)_{\rm SFD}$. In Figure 5, the derived color excesses of various colors are plotted against the derived $E(B-V)$ for the target stars, and the corresponding reddening coefficients relative to $E(B-V)$ were derived following the same procedure as in Figure 4. Again, the R^2 values of the linear fits for all the colors are greater than 0.98.

In Table 3, we summarize the derived reddening/extinction coefficients for various colors/bands. The reddening/extinction coefficients relative to $E(B-V)_{\rm SFD}$ are denoted with the superscript "SFD" to be distinguished from those relative to $E(B-V)$. The extinction coefficients for the bands, i.e., R_a and $R_a^{\rm SFD}$, were simply calculated from the derived R_{a-b} and $R_{a-b}^{\rm SFD}$ assuming $R_V = 3.1$ and $R_V^{\rm SFD} = 3.1 \times 0.78$.

3.2. Comparison with Results from Extinction Laws

For comparison, we also list in Table 3 the reddening/extinction coefficients predicted by the extinction laws of Fitzpatrick (1999), Cardelli et al. (1989, CCM) and O'Donnell (1994). They were calculated based on the corresponding $R_V = 3.1$ extinction curves in combination with the photonic passbands[9] and a source spectrum of G0V star[10] at $E(B-V) = 0.4$ mag.

As displayed in Table 3, reddening coefficients for the $u-v$ color predicted by the three extinction laws are apparently different from each other, and our result is closest to that given by the CCM extinction law. For the $v-g$ color, the reddening coefficient predicted by CCM is obviously larger than those of the other two extinction laws, but is still significantly smaller than that derived in this work. For the $g-r$, $i-z$ and $V-r$ colors, the reddening coefficients derived in this work are most consistent with those predicted by the Fitzpatrick extinction law, while for the $r-i$ and $z-y$ colors, our results favor the CCM and O'Donnell extinction laws, respectively.

3.3. Variations

The target sample employed to derive reddening coefficients covers a wide range of effective temperatures (∼4000–8000 K). To investigate whether the derived reddening coefficients vary with effective temperatures, we divided the sample into several groups at intervals of 500 K. For each group, reddening coefficients were derived using the same procedure described above. The results affirm that variations of reddening coefficients with effective temperatures do not exceed 0.1 for all the colors, e.g., $R_{u-v}^{\rm SFD}$ varies between 0.25 and 0.267, and $R_{v-g}^{\rm SFD}$ varies between 1.027 and 1.117. Moreover, for all the colors, no obvious trends were found between reddening coefficients and effective temperatures.

We also investigated variations of the derived reddening coefficients with $E(B-V)_{\rm SFD}$ by plotting $E(a-b)/E(B-V)_{\rm SFD}$ against $E(B-V)_{\rm SFD}$ for each color of the target stars. Figure 6 shows the cases of $u-v$ and $v-g$ as two typical examples. The data points within the range $0.1\ {\rm mag} < E(B-V)_{\rm SFD} < 0.7$ mag were binned into six groups with a bin size of 0.1 mag. The median value of each group is signified with a vermilion plus in the plot. The vermilion line represents the best linear fit to the six median points. The slope and associated uncertainty of the linear fit are marked at the top right of each panel. All the colors exhibit decline trends (i.e., negative slopes) of $E(a-b)/E(B-V)_{\rm SFD}$ with increasing $E(B-V)_{\rm SFD}$. The $v-g$ and $g-r$ colors show the most prominent decline trends, for which the slopes of the linear fits are −0.34 and −0.18, respectively, while for the other colors, the corresponding slopes are between −0.1 and 0. As the $v-g$ and $g-r$ colors also have the largest reddening coefficients, if measured in relative amplitude, the variations of reddening coefficients from $E(B-V)_{\rm SFD} \sim 0$ to 1 are of the same order (between 20 and 30 percent) for all the colors except $r-i$, for which the relative variation of reddening coefficient is 11 percent.

[9] Photonic passbands for the SAGES and Pan-STARRS systems were from this work and Tonry et al. (2012), respectively.

[10] The spectrum "ings_025_g0v.dat" from the INGS library was adopted here.

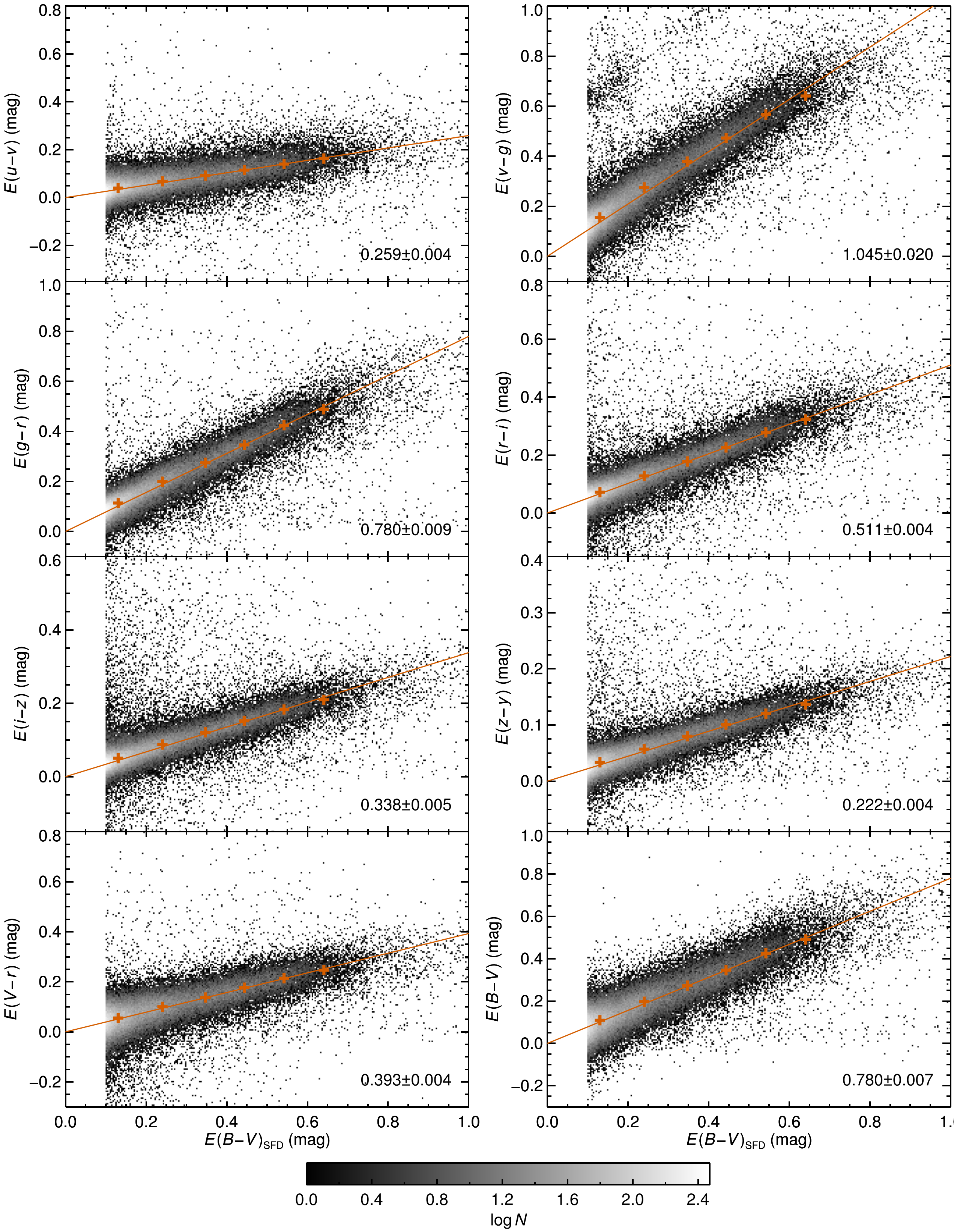

Figure 4. Color excesses of $u-v$, $v-g$, $g-r$, $r-i$, $i-z$, $z-y$, $V-r$ and B–V as a function of $E(B-V)_{\rm SFD}$ for the target stars. The data points within the range 0.1 mag $< E(B-V)_{\rm SFD} <$ 0.7 mag are binned into six groups with a bin size of 0.1 mag, and the median value of each group is signified with a vermilion plus. The vermilion line represents the best linear fit (through the origin) to the six median points, and the slope is marked at the bottom right of each panel.

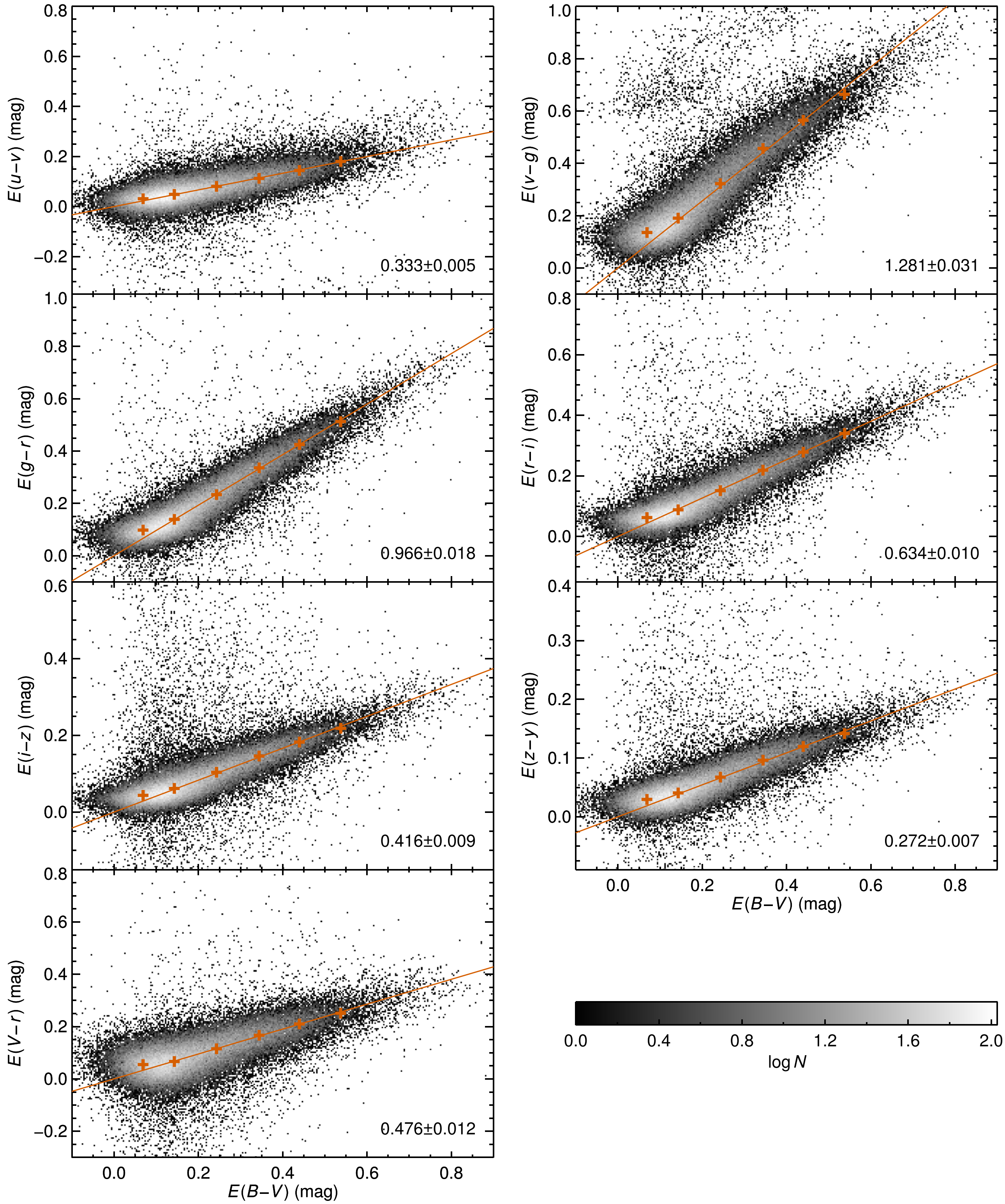

Figure 5. Color excesses of $u-v$, $v-g$, $g-r$, $r-i$, $i-z$, $z-y$ and $V-r$ as a function of $E(B-V)$ for the target stars. The symbols and lines are similar to those in Figure 4 except that the binning range for $E(B-V)$ is 0–0.6 mag.

Table 3
Reddening/Extinction Coefficients for Various Colors/Bands

	This Work	This Work	Fitzpatrick	CCM	O'Donnell
Color	$R^{\rm SFD}_{a-b}$		R_{a-b}		
$u-v$	0.259 ± 0.004	0.333 ± 0.005	0.460	0.378	0.530
$v-g$	1.045 ± 0.020	1.281 ± 0.031	0.881	0.979	0.838
$g-r$	0.780 ± 0.009	0.966 ± 0.018	0.989	0.873	0.916
$r-i$	0.511 ± 0.004	0.634 ± 0.010	0.663	0.640	0.593
$i-z$	0.338 ± 0.005	0.416 ± 0.009	0.402	0.475	0.492
$z-y$	0.222 ± 0.004	0.272 ± 0.007	0.247	0.258	0.268
$V-r$	0.393 ± 0.004	0.476 ± 0.012	0.474	0.399	0.421
Band	$R^{\rm SFD}_{a}$		R_{a}		
u	4.109 ± 0.004	5.204 ± 0.005	4.894	4.938	4.972
v	3.850 ± 0.020	4.871 ± 0.031	4.434	4.560	4.442
g	2.805 ± 0.009	3.590 ± 0.018	3.553	3.581	3.604
r	2.025 ± 0.004	2.624 ± 0.012	2.564	2.708	2.688
i	1.514 ± 0.004	1.990 ± 0.010	1.901	2.068	2.095
z	1.176 ± 0.005	1.574 ± 0.009	1.499	1.593	1.603
y	0.954 ± 0.004	1.302 ± 0.007	1.252	1.335	1.335

Note. The second and third columns are our reddening/extinction coefficients derived relative to $E(B-V)_{\rm SFD}$ and $E(B-V)$, respectively. The fourth to sixth columns are reddening/extinction coefficients predicted by the extinction laws of Fitzpatrick, CCM and O'Donnell, respectively.

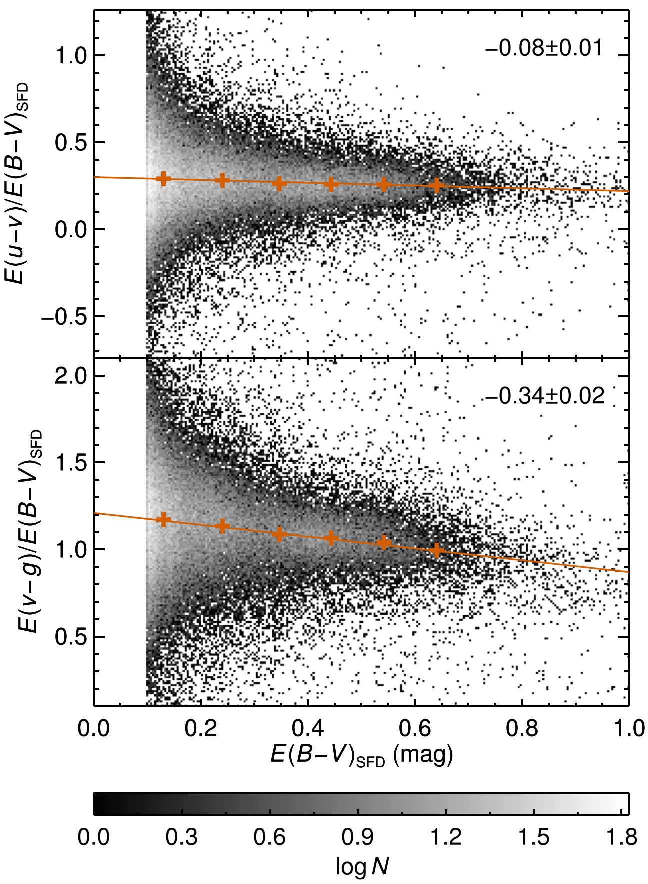

Figure 6. $E(a-b)/E(B-V)_{\rm SFD}$ for $u-v$ (top) and $v-g$ (bottom) as a function of $E(B-V)_{\rm SFD}$ for the target stars. The symbols and lines are similar to those in Figure 4.

4. Summary

The SAGES is a multi-band photometric survey focused on estimation of stellar atmospheric parameters and interstellar extinction. Observations for the SAGES u and v bands have been done with the Bok Telescope on Kitt Peak, and the data have been reduced and internally released.

We have derived photonic passbands for the SAGES u and v bands by convolving the filter transmissions with the CCD quantum efficiency and an atmospheric transmission of one air mass. Comparisons with the Strömgren and the SkyMapper photometric systems show that the SAGES u band has very similar characteristic wavelengths ($\lambda_{\rm mean}$ and $\lambda_{\rm pivot}$) to the Strömgren/SkyMapper u bands, but its bandwidth is the narrowest among the three systems. For the v bands, both the characteristic wavelengths and bandwidth of the SAGES system are in between those of the Strömgren and the SkyMapper systems. The validity of the derived photonic passbands has been verified by comparing synthetic/hybrid color–color diagrams with the observed ones, and the results show that they could reproduce the observations very well.

We have also derived observed, model-free extinction coefficients for the SAGES u and v bands using the "standard pair" method. As the SAGES u and v bands were devised to be used together with the Pan-STARRS photometric data, extinction coefficients for the Pan-STARRS g, r, i, z and y bands have also been derived using the same method. Our results confirm that interstellar extinction given by SFD is overestimated, and hence two sets of extinction coefficients have been derived, one set relative to $E(B-V)_{\rm SFD}$ and the other relative to the intrinsic $E(B-V)$. We have compared the reddening coefficients derived in this work with those predicted by the Fitzpatrick, CCM and O'Donnell extinction laws, and none of them could reproduce our results for all the colors. We have also investigated the variations of reddening coefficients with effective temperatures and $E(B-V)_{\rm SFD}$. No obvious trends or significant variations with effective temperatures have been found, but reddening coefficients for all the colors show decline trends with increasing $E(B-V)_{\rm SFD}$, with typical relative variations of twenty-some percent from $E(B-V)_{\rm SFD} \sim 0$ to 1.

Acknowledgments

We would like to thank the referee for the valuable suggestions and comments. This work is supported by the National Natural Science Foundation of China (NSFC, Grant Nos. 11988101, 12090044, 12090040, 11673030, 42075123 and 62127901), and the National Key R&D Program of China under grant No. 2019YFA0405502. We acknowledge the science research grants from the China Manned Space Project with No. CMS-CSST-2021-B05. The Guoshoujing Telescope (the Large Sky Area Multi-Object Fiber Spectroscopic Telescope, LAMOST) is a National Major Scientific Project built by the Chinese Academy of Sciences. Funding for the project has been provided by the National Development and Reform Commission. LAMOST is operated and managed by the National Astronomical Observatories, Chinese Academy of Sciences. This work has made use of data from the European Space Agency (ESA) mission Gaia (https://www.cosmos.esa.int/gaia), processed by the Gaia Data Processing and Analysis Consortium (DPAC, https://www.cosmos.esa.int/web/gaia/dpac/consortium). Funding for the DPAC has been provided by national institutions, in particular the institutions participating in the Gaia Multilateral Agreement. The Pan-STARRS1 Surveys (PS1) and the PS1 public science archive have been made possible through contributions by the Institute for Astronomy, the University of Hawaii, the Pan-STARRS Project Office, the Max-Planck Society and its participating institutes, the Max Planck Institute for Astronomy, Heidelberg and the Max Planck Institute for Extraterrestrial Physics, Garching, The Johns Hopkins University, Durham University, the University of Edinburgh, the Queen's University Belfast, the Harvard-Smithsonian Center for Astrophysics, the Las Cumbres Observatory Global Telescope Network Incorporated, the Central University of Taiwan (China), the Space Telescope Science Institute, the National Aeronautics and Space Administration under Grant No. NNX08AR22G issued through the Planetary Science Division of the NASA Science Mission Directorate, the National Science Foundation grant No. AST-1238877, the University of Maryland, Eotvos Lorand University (ELTE), the Los Alamos National Laboratory, and the Gordon and Betty Moore Foundation. This research has made use of the APASS database, located at the AAVSO website. Funding for APASS has been provided by the Robert Martin Ayers Sciences Fund. This research has made use of the VizieR catalog access tool, CDS, Strasbourg, France (DOI:10.26093/cds/vizier), the TOPCAT (http://www.starlink.ac.uk/topcat/; Taylor 2005) software, and the NASA's Astrophysics Data System.

ORCID iDs

Ke-Feng Tan https://orcid.org/0000-0003-0173-6397
Gang Zhao https://orcid.org/0000-0002-8980-945X
Zhou Fan https://orcid.org/0000-0002-6790-2397
Wei Wang https://orcid.org/0000-0002-9702-4441
Hai-Bo Yuan https://orcid.org/0000-0003-2471-2363
Jie Zheng https://orcid.org/0000-0001-6637-6973
Nan Song https://orcid.org/0000-0002-2241-7945
Jing-Kun Zhao https://orcid.org/0000-0003-2868-8276

References

Bessell, M., Bloxham, G., Schmidt, B., et al. 2011, PASP, 123, 789
Bessell, M. S. 2011, PASP, 123, 1442
Cardelli, J. A., Clayton, G. C., & Mathis, J. S. 1989, ApJ, 345, 245
Chambers, K. C., Magnier, E. A., Metcalfe, N., et al. 2016, arXiv:1612.05560
Cui, X.-Q., Zhao, Y.-H., Chu, Y.-Q., et al. 2012, RAA, 12, 1197
Evans, D. W., Riello, M., De Angeli, F., et al. 2018, A&A, 616, A4
Fan, Z., Zhao, G., Wang, W., et al. 2018, Progress in Astronomy, 36, 101
Fitzpatrick, E. L. 1999, PASP, 111, 63
Flewelling, H. A., Magnier, E. A., Chambers, K. C., et al. 2020, ApJS, 251, 7
Gaia Collaboration, Brown, A. G. A., Vallenari, A., et al. 2018, A&A, 616, A1
Gaia Collaboration, Prusti, T., de Bruijne, J. H. J., et al. 2016, A&A, 595, A1
Gregg, M. D., Silva, D., Rayner, J., et al. 2006, in The 2005 HST Calibration Workshop: Hubble After the Transition to Two-Gyro Mode, ed. A. M. Koekemoer, P. Goudfrooij, & L. L. Dressel, 209
Heap, S. R., & Lindler, D. J. 2007, in ASP Conf. Ser., 374, From Stars to Galaxies: Building the Pieces to Build Up the Universe, ed. A. Vallenari et al. (San Francisco, CA: ASP), 409
Henden, A. A., Welch, D. L., Terrell, D., & Levine, S. E. 2009, BAAS, 41, 669
Keller, S. C., Schmidt, B. P., Bessell, M. S., et al. 2007, PASA, 24, 1
Koleva, M., & Vazdekis, A. 2012, A&A, 538, A143
O'Donnell, J. E. 1994, ApJ, 422, 158
Pickles, A. J. 1998, PASP, 110, 863
Schlafly, E. F., & Finkbeiner, D. P. 2011, ApJ, 737, 103
Schlafly, E. F., Finkbeiner, D. P., Schlegel, D. J., et al. 2010, ApJ, 725, 1175
Schlegel, D. J., Finkbeiner, D. P., & Davis, M. 1998, ApJ, 500, 525
Strömgren, B. 1966, ARA&A, 4, 433
Taylor, M. B. 2005, in ASP Conf. Ser., 347, Astronomical Data Analysis Software and Systems XIV, ed. P. Shopbell, M. Britton, & R. Ebert (San Francisco, CA: ASP), 29
Tonry, J. L., Stubbs, C. W., Lykke, K. R., et al. 2012, ApJ, 750, 99
Wang, W., Zhao, G., Chen, Y., & Liu, Y. 2014, Setting the scene for Gaia and LAMOST, in Proc. Int. Astronomical Union, Symp. S298, ed. S. Feltzing et al., 326
Yuan, H. B., Liu, X. W., & Xiang, M. S. 2013, MNRAS, 430, 2188
Zhao, G., Chen, Y.-Q., Shi, J.-R., et al. 2006, ChJAA, 6, 265
Zhao, G., Zhao, Y.-H., Chu, Y.-Q., Jing, Y.-P., & Deng, L.-C. 2012, RAA, 12, 723
Zheng, J., Zhao, G., Wang, W., et al. 2018, RAA, 18, 147
Zheng, J., Zhao, G., Wang, W., et al. 2019, RAA, 19, 003